# Synthesis of poly(1-vinylimidazole)-block-poly(9-vinylcarbazole) copolymers via RAFT and their use in chemically responsive graphitic composites

Migliore, Nicola; Araya-Hermosilla, Esteban; Scheutz, Georg M.; Sumerlin, Brent S.; Pucci, Andrea; Raffa, Patrizio

*Published in:*
Journal of Polymer Science

*DOI:*
10.1002/pol.20210736

Received: 1 October 2021 | Revised: 17 November 2021 | Accepted: 21 November 2021

DOI: 10.1002/pol.20210736

RESEARCH ARTICLE

JOURNAL OF POLYMER SCIENCE WILEY

# Synthesis of poly(1-vinylimidazole)-*block*-poly (9-vinylcarbazole) copolymers via RAFT and their use in chemically responsive graphitic composites

**Nicola Migliore**[1,2] | **Esteban Araya-Hermosilla**[3] | **Georg M. Scheutz**[2] | **Brent S. Sumerlin**[2] | **Andrea Pucci**[4,5] | **Patrizio Raffa**[1]

[1]Department of Chemical Engineering, ENTEG Institute, Faculty of Science and Engineering, University of Groningen, Groningen, The Netherlands

[2]George & Josephine Butler Polymer Research Laboratory, Department of Chemistry, University of Florida, Gainesville, Florida, USA

[3]Center for Micro-BioRobotics, Istituto Italiano di Tecnologia, Pontedera, Italy

[4]Department of Chemistry and Industrial Chemistry, University of Pisa, Pisa, Italy

[5]CISUP, Centro per l'Integrazione della Strumentazione dell'Università di Pisa, Pisa, Italy

**Correspondence**
Patrizio Raffa, Department of Chemical Engineering, ENTEG Institute, Faculty of Science and Engineering, University of Groningen, Nijenborgh 4 9747 AG, Groningen, The Netherlands.
Email: p.raffa@rug.nl

**Funding information**
University of Pisa

**Abstract**

This study reports the synthesis of novel poly(1-vinylimidazole)-*b*-poly(9-vinylcarbazole) (PVI-*b*-PVK) block copolymers with varying monomer ratios using reversible addition-fragmentation chain-transfer (RAFT) polymerization and their incorporation in responsive composite materials. Specifically, non-covalent exfoliation of two different conductive fillers, multi-walled carbon nanotubes (MWCNTs) or reduced graphene oxide (rGO), was studied. The percolation threshold of the synthesized nanocomposites was dependent on the polymer used for dispersion, showing a better affinity of the fillers for block copolymers with higher relative carbazole content. Resistivity measurements showed selective variation in the resistance signal when the materials were exposed to various organic solvents and acids, providing a good basis for the design of sensing devices.

**KEYWORDS**

block copolymers, chemical sensors, nanocomposites, RAFT, responsive materials

## 1 | INTRODUCTION

Stimuli-responsive polymers have the ability to change morphologies and properties in different environments once they are exposed to an external stimulus, such as a change in temperature, pH, or light wavelength.[1–3] Additionally, remarkable results have been recently achieved in their synthesis using living polymerization techniques, including reversible addition-fragmentation chain-transfer (RAFT) polymerization.[4–6] Furthermore, their use in combination with graphitic fillers (GF) allows straightforward access to responsive and conductive nanocomposites. The latter display broad applicability as, for example, molecular wires, molecular electronics, probes, high-strength fibers, field emission devices,[7–13] and as analytical sensors.[14–22]

One of the problems connected to the use of GF in the synthesis of conductive nanocomposites is the tendency to remain in a strongly aggregated state, which makes it very difficult to obtain an effective dispersion inside a polymer matrix.[23,24] To facilitate the dispersion, it is possible to increase the GF affinity for the matrix using two alternative approaches, namely covalent or non-covalent dispersion. Covalent dispersion is based on the covalent bonding between a stabilizing matrix—typically a polymer—and the GF. For example, treating carbon nanotubes (CNTs) with strong acid can generate structural defects for anchoring of azide groups that serve as reactive sites for polymers containing alkyne groups.[25,26] As another example, there are several reports of functionalizing CNTs with bromide derivates[6,27] or RAFT agents[28–30] to graft polymer chains directly from the surface of CNTs. However, covalent interactions inevitably affect the physical properties of GF due to the resulting interference with the $\pi$-conjugation of GF. Even so, the covalent approach is still highly valuable, due to its efficient exfoliation of GF bundles and the ability to successfully disperse GF in the polymer matrix.

In the case of the non-covalent approach, interactions such as $\pi$-$\pi$ or H-bonding are used to disperse GF without modifying the structural integrity of the GF.[31] Contrary to covalent methods, the stability of the resulting dispersions is often compromised over time. It has been reported that the nondestructive functionalization of CNTs can be achieved by coating the CNTs followed by a polymerization step.[32,33] Likewise, several papers have reported the functionalization of polymers and subsequent non-covalent grafting using aromatic structures, such as pyrene, styrene, or perylene derivates.[34–36]

Among the polymers that have been used for non-covalent dispersion of GF, poly(*9*-vinylcarbazole) (PVK) has shown outstanding results.[37–39] Specifically, the combination of PVK and GF makes it an interesting nanocomposite material for the development of practical semiconductor devices. Besides the ability to efficiently exfoliate GF via $\pi$-$\pi$ interactions, the carbazole moieties can behave as electron donors, exchanging electrons with the CNTs to form the corresponding charged counterions and extending their electro-optical properties.[37,40,41] For example, Aydin et al. synthesized a nanocomposite of PVK and graphene oxide (GO), obtaining a material that displayed good conductivity properties.[42] Similar results were obtained by preparing conductive nanocomposite but using reduced GO (rGO) instead of the normal GO.[43,44] Advincula et al. has reported the preparation of PVK-CNTs nanocomposites dispersions that showed good stability for an extended time period (months) without any precipitation of CNTs, suggesting PVK is a suitable matrix for conductive nanocomposites.[37]

Another interesting polymer that has been used for the dispersion of GF is PVI.[45,46] The imidazole ring can form intermolecular H-bonding between the GF and the polymer, resulting in a stable dispersion. In addition, the imidazole is known for its sensitivity to analytes that are capable of forming H-bonds and coordinate (in the case of metal ions) with imidazole rings. This characteristic renders PVI well-suited for the synthesis of biosensors[47–52] and membranes for metal ion complexing and removal.[53,54] Additionally, imidazole is a weak base,[55–59] making it a good candidate for acid-sensing devices.

Given the findings of these previous reports, we hypothesized that the synthesis of copolymers containing PVK and PVI could comprise versatile systems for the preparation of analytical devices. While copolymerization of 9-vinylcarbazole (VK) with other monomers has been shown,[46] the merging of PVK and PVI in a controlled block copolymerization has yet to be achieved. Access to such copolymer architectures would provide excellent properties for the generation of conductive and responsive GF materials, where the PVK block can help to produce highly exfoliated conductive nanocomposites,[37] and PVI provides stimuli responsiveness.

In this study, amphiphilic copolymers of PVI-*b*-PVK were synthesized via controlled radical polymerization and used as polymer matrices for the preparation of stimuli-responsive nanocomposites. The nanocomposites were tested for the detection of chlorinated solvents and organic acids. RAFT polymerization was used to obtain block copolymers with different VI/VK ratios. The copolymers were characterized by $^1$H-NMR spectroscopy, gel permeation chromatography (GPC), differential scanning calorimetry (DSC), and UV–Vis and fluorescence spectroscopy. In addition, two different nanocomposites were prepared by non-covalent dispersion of multi-walled carbon nanotubes (MWCNTs) or reduced graphene oxide (rGO). The final nanocomposites were characterized by thermal gravimetric analysis (TGA) to evaluate the amount of the graphitic filler (GF) dispersed, and by resistance measurements to quantify their conductivity. Finally, the best nanocomposite was studied and compared with the respective homopolymer-based nanocomposites (PVI and PVK) to evaluate the role of the single blocks on the final properties of the material.

## 2 | RESULTS AND DISCUSSION

### 2.1 | Synthesis and polymer characterization

Initially, various macroRAFT agents of PVK and PVI homopolymers having different length were synthesized

by RAFT. Reaction schemes are reported in the experimental section at the end of the manuscript. One macroRAFT agent was selected for subsequent chain extension and block copolymer formation. The conditions and results are summarized in Table 1. It should be mentioned that VI is a less active monomer (LAM) in RAFT, since radicals generated during polymerization cannot form resonance structures with the heterocyclic ring, making it challenging to polymerize.[60] It has been recently shown that imidazole monomers can be polymerized via RAFT with good results using glacial acetic acid as solvent,[60,61] therefore, we followed this approach.

As reported in Table 1, the use of the methyl 2-(butylthiocarbonothioylthio)propanoate trithiocarbonate (MCEBTTC) as the RAFT agent gave narrow dispersity and good yield in the synthesis of PVI. This RAFT agent is almost identical to the agent used in a previous report about VI-based RAFT polymers, except for the substitution of the terminal acid group with an ester one.[60] Three

**TABLE 1** Conditions and results of the polymerizations carried out in this work

| Sample name | $t$ (h) | Conv[a] (%) | $[M]_0$:$[CTA]_0$:$[I]_0$ | $M_n^{theo}$ (g·Mol$^{-1}$)[b] × $10^3$ | $M_n^{exp}$ (g·Mol$^{-1}$) × $10^3$ | $Đ$ |
|---|---|---|---|---|---|---|
| PVI 6 k | 22 | 90 | 151:2:1 | 5.9 | 5.7[c] | 1.29 |
| PVI 12 k | 22 | 70 | 265:2:1 | 9.1 | 8.5[c] | 1.30 |
| PVI 21 k | 22 | 51 | 424:2:1 | 11.0 | 10.6[c] | 1.41 |
| PVK 10 k | 7 | 74 | 110:2:1 | 7.7 | 3.2[d] | 1.10 |
| PVK 20 k | 7 | 66 | 206:2:1 | 14.1 | 7.6[d] | 1.37 |
| PVK 30 k | 23[e] | 61 | 360:2:1 | 18.6 | 7.0[d] | 1.58 |
| PVI 6 k-*b*-PVK | 23 | 60 | 246:2:1 | 20.1 | 8.9[c] | 1.61 |
| PVI 12 k-*b*-PVK | 23 | 68 | 200:2:1 | 23.0 | 11.6[c] | 1.51 |
| PVI 21 k-*b*-PVK | 23 | 39 | 170:2:1 | 16.7 | 11.0[c] | 1.47 |

[a]Conversions were determined by $^1$H-NMR spectroscopy (spectra reported in the SIc.
[b]$M_n$ (theoryc at experimental conv values.
[c]Based on conventional calibration with PS standards.
[d]Based on conventional calibration with Pullulan standards.
[e]Longer polymerization time used, due to an initial inhibition period.

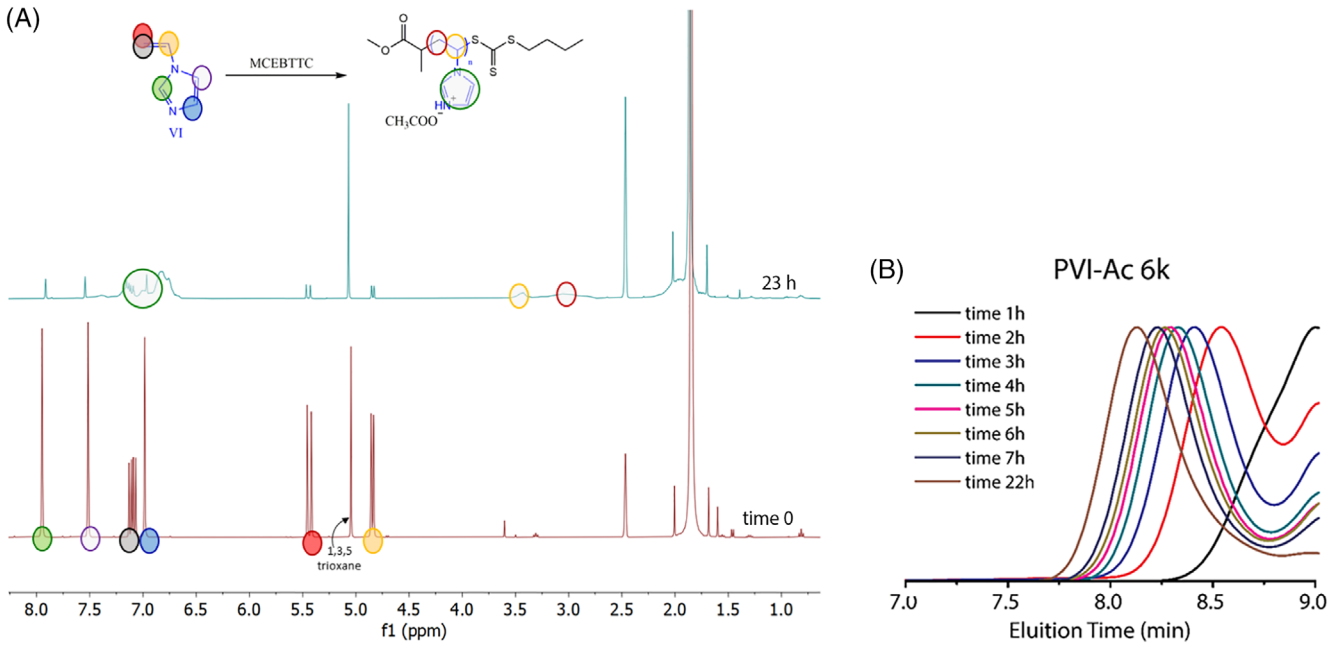


**FIGURE 1** (A) $^1$H-NMR traces comparison of PVI-Ac-6 k. (B) GPC traces obtained in DMF of the kinetic studies of PVI-Ac-6 k shown as example for the PVI polymerization

different PVI macroRAFT agents were synthesized with different $M_n$ to evaluate the molecular weight effect of PVI during the synthesis and on the final properties of the nanocomposites with different GF.

The polymerization kinetics of VI was studied by $^1$H-NMR spectroscopy (Figures 1A and S3) and GPC (Figures 1B and S4). The $^1$H-NMR traces (Figure 1A) display a decrease of the signals associated with the imidazole vinyl bond (~7.2, ~5.5, and ~4.8 ppm) over time, and the appearance of new signals (between 3.6 and 2.8 ppm) associated to the -CH- and -$CH_2$- of the polymer backbone.

The plot of $\ln([M]_0/[M]_t)$ as function of time displays a linear increase, thus indicating pseudo-first-order kinetics, indicative of a steady-state radical concentration. An inflection of the curve is observed at relatively longer times ($t > 7$ h, Figure 2A), indicating decreased radical concentration, most likely due to termination events and the depletion of initiator. The slope of $\ln([M]_0/[M]_t)$ versus polymerization time decreased with increasing target molecular weight probably due to the lower AIBN concentrations in these polymerizations. The total monomer concentration was kept constant, while the ratio of monomer to AIBN increased, resulting in a lower AIBN concentration for these polymerizations. It may be noticed here that the conversions and final molecular weights obtained in the kinetics experiments, differ slightly from those reported in Table 1, despite the reaction being performed in the same conditions. This may indicate some effect due to the different scale at which the reactions were performed, or generally lower reproducibility, but we did not further investigate it.

The GPC chromatogram over time displays monomodal peaks that shift to lower retention volume, indicating a uniform growth of the polymer chains (Figures 1B and S4).

The molecular weights of the different PVI macroRAFT synthesized in this work increased with conversion, typical of a living system, as shown in Figure 2B. It needs to be mentioned that $Đ$ increased slightly with the polymerization progress for all the polymerizations, however, the final $Đ$ values remained below 1.3 (except for PVI 21 K which displays slightly higher $Đ \sim 1.4$). This is in line with a previous report of VI RAFT polymerization that showed broader molecular weight distributions above 60% conversion.[60] For all polymerization experiments, we observed a deviation of the measured $M_n$ values as function of the conversion from the theoretical $M_n$ ones. This behavior could be explained by the fact that $M_n$ was obtained from Pullulan standards that likely show a different hydrodynamic volume compared to PVI. However, those results are comparable to a previous report.[60]

Furthermore, macroRAFT agents of PVK characterized by different molecular weights were also synthesized (Table 1). The success of the polymerization was proven by $^1$H-NMR spectroscopy (Figure S5) and by GPC (Figure S6). After both macroRAFT agent types were successfully synthesized and characterized, they were evaluated for their chain extension performance to prepare the final diblock copolymers of VI and VK. The chain extension of PVK in DMF was unsuccessful due to a precipitate formation after a short time. The symmetric approach, i.e. chain extension of PVI with VK, was then

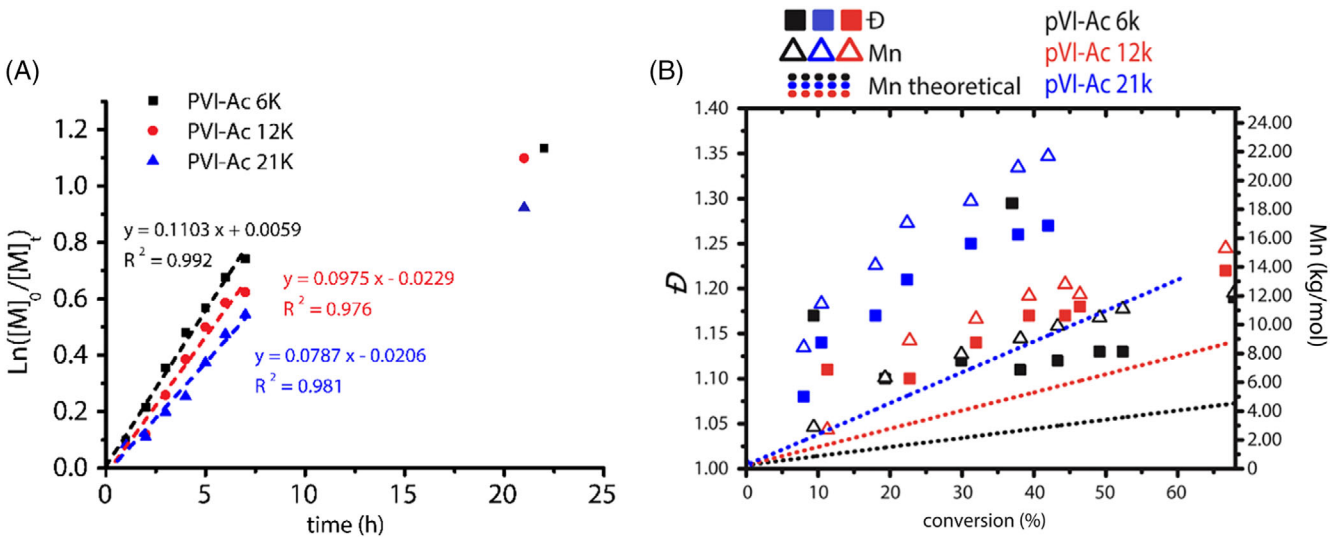


FIGURE 2 (A) Kinetics study of PVI macroRAFT agents at different target $M_n$ (6 kg/Mol, 12 kg/Mol and 21 kg/Mol) via thermo-initiated RAFT. (B) Comparison of the corresponding $M_n$ (6 kg/Mol, 12 kg/Mol, and 21 kg/Mol), $Đ$ and theoretical molecular weight evolutions over conversion

chosen. The kinetic study of the PVI chain extension using VK was again studied by $^1$H-NMR spectroscopy (Figures 3A and S7) and by GPC (Figures 3B and S8). The $^1$H-NMR spectra display a decreasing of the signals associated with the carbazole vinyl bond (~5.6 and ~5.1 ppm) and the appearance of new signals (between 3.6 and 2.0 ppm) associated with the -CH- and -$CH_2$- of the polymer backbone. Moreover, it is possible to observe broad signals between ~7.0 and ~5.8 ppm that are assigned to the carbazole protons of the PVK block.

The kinetic plot shows a very reasonable fit with a pseudo-first-order kinetics (Figure 4A), with the slight

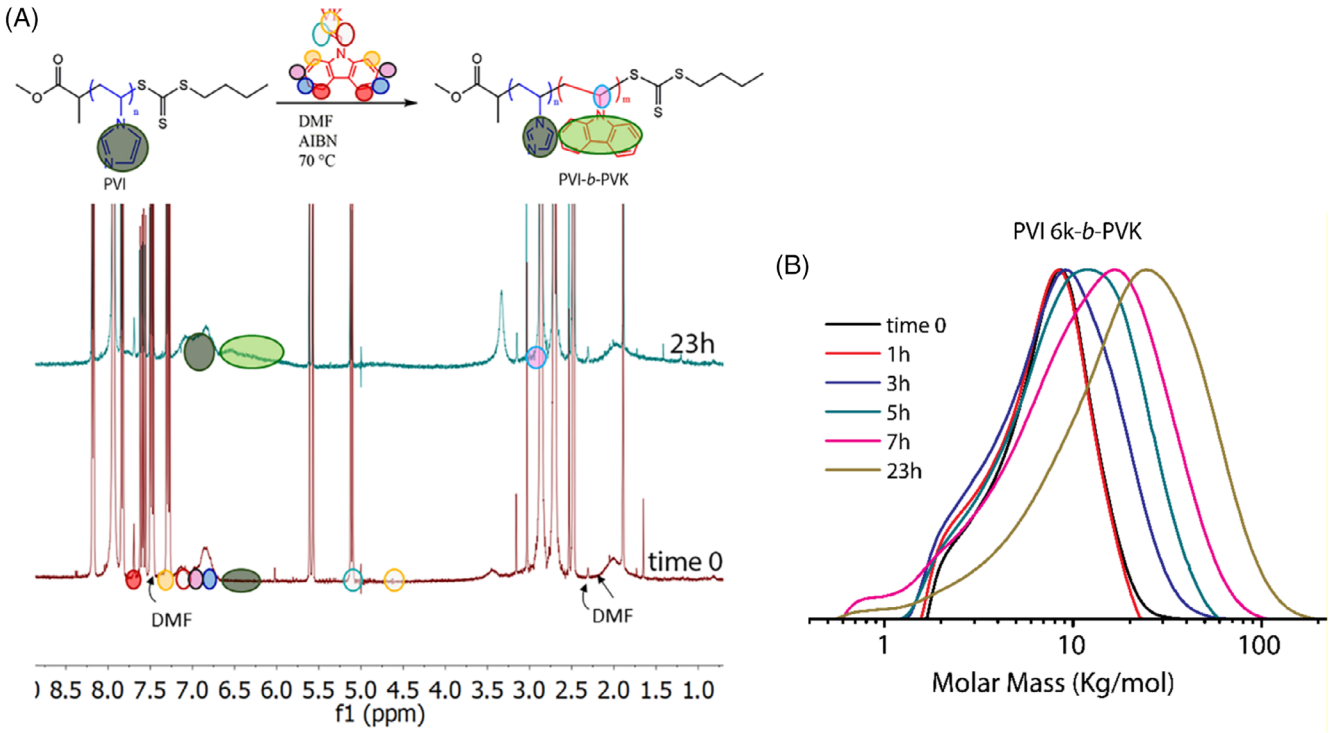


**FIGURE 3** (A) $^1$H-NMR traces of the chain extension reaction of PVI-Ac-6 k and (B) GPC traces obtained in DMF of the kinetic studies of PVI 6 k-*b*-PVK shown as example for the chain extension reactions of this work

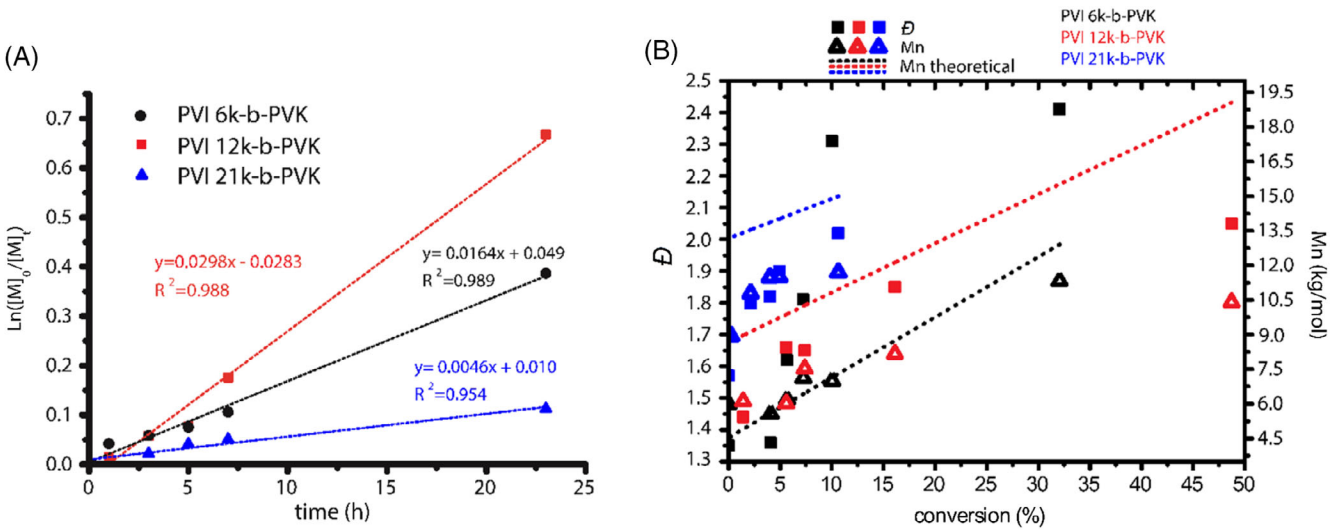


**FIGURE 4** (A) Kinetics study of chain extension of PVI macroRAFT agents with VK at different target $M_n$ via RAFT. (B) Comparison of the corresponding $M_n$, $Đ$ and theoretical molecular weight evolutions over conversions for different PVI-*b*-PVK

deviation from the linear fit being an indication of different polymerization behavior (or experimental uncertainty). PVI 6 k-b-PVK has a lower polymerization rate than PVI 12 k-b-PVK, probably because of a lower number of MCEBTTC-terminated chains, despite a higher monomer/initiator ratio.

As shown in the GPC chromatogram in Figure S10, the polymer peaks shift to higher $M_n$ over time, despite a small tail probably due to the presence of dead PVI chains. Moreover, if the $M_n$ is plotted as function of conversion, it increases linearly as shown in Figure 4B, except PVI 21 k-b-PVK, where the $M_n$ reaches a plateau around 7% of the conversion value. The increase of $Đ$ values could be attributed to a combination of chain-chain recombination side-reactions and due to the fact that some polymer chains are not RAFT agent terminated.

As matter of fact, the control on the synthesized copolymers resulted to be poor. Indeed, despite the GPC traces (Figures 3B and S8) for all the copolymers shift to higher molar mass compared to the corresponding macroinitiators, the presence of tails and bimodal peaks suggests a poor control. Although the synthesis was not optimized, the results show that block structures were successfully obtained, thus the polymers were used to prepare the intended nanocomposites, which represents the main focus of this work.

Once the kinetic studies of macroRAFT agents and their chain extension were carried out a larger batch of polymers (~5 g each of the final polymers) was synthesized and characterized by $^1$H-NMR spectroscopy, GPC, and DSC analysis (Figures S9, S10, and S11) in order to get enough material for the preparation and characterization of the conductive nanocomposites. As reported above, the polymers obtained have slightly different $M_n$, $Đ$, and conversion values than the one used to study their kinetics.

To evaluate the effect of the block copolymer composition on the dispersion of GF, it is important to estimate the monomer molar ratio VI/VK. Unfortunately, this was difficult to estimate by $^1$H-NMR spectroscopy, since the signals of VI and VK rings are mostly overlapped. However, based on the GPC analysis in DMSO (Figure S10), it was possible to estimate the ratio VI/VK as reported in Table S3.

Finally, since carbazole-derivate polymers are known for their optical features, to give a full characterization of these new materials, some spectroscopic properties of interest were measured as reported in the supporting information of this work. The results show that the presence of carbazole groups render all the prepared materials fluorescent, behaving similarly to what reported in literature for analogous polymers.[62–64]

## 2.2 | Preparation of electrically conductive rGO/polymer composites

Dispersions of the GFs rGO and MWCNTs in PVI 6 k, PVK 10 k and PVI 6 k-*b*-PVK polymers were made in NMP mixing 30 mg of GF and 110 mg of polymer following the procedure reported in the experimental section of this work. Some considerations can be drawn from the TGA curves comparison between the pristine polymers and their composites. Notably, the polymers PVI and PVI-*b*-PVK showed 5 wt% mass loss at 160 °C, instead PVK was stable up to 350 °C with the same mass loss (Figure S14a). Moreover, as shown by the first derivative of the thermogravimetric curves in Figure S14b, the PVI and PVI-*b*-PVK show two different temperature regions for degradation. The PVI shows the first degradation step around 180 °C and the second around 450 °C. Instead, for PVI-*b*-PVK two degradation temperatures around 450 °C and 490 °C were observed. Since the PVK homopolymer displays one degradation temperature at 470 °C, we assumed that the first degradation temperature for the PVI-*b*-PVK is mainly associated with the PVI block and the second one to the PVK block. Of course, thermal degradation is a much more complex phenomenon, and the two blocks likely influence each other. However, based on this assumption, we tried to qualitatively estimate the VI/VK ratio in the synthetized copolymers. It is interesting to notice that the ratio VI/VK based on the TGA analysis seems to have the same trend of the same ratio obtained by GPC Table S3.

Another important result gathered from the TGA investigation was the thermal stabilization of the nanocomposites compared to the pristine copolymers. It was worth noting that the scavenging characteristics of MWCNTs[65] delayed the initial thermal degradation of the nanocomposite by approximately 200 °C, while the use of rGO pushed the initial thermal degradation of the nanocomposites by approximately 150 °C. However, this enhancement in polymer stability was not observed for the second degradation steps of both polymers (PVI 6 k and PVI 6 k-*b*-PVK).

We evaluated the amount of polymer interacting with the GF by TGA (Figure 5). Comparing the final residue of PVI 6 k and PVI 6 k-b-PVK before and after the dispersion of GF, it is possible to estimate the amount of polymer that interacted with the GF after the filler dispersion step.

Table 2 shows that the PVI 6 k seems to interact more with rGO than MWCNTs, as indicated in the higher mass loss (10.9 against 8.0 wt%). Conversely, PVI 6 k-*b*-PVK shows an opposite trend because the PVK block helps to create stronger interactions with MWCNTs (about 26 wt % against 7.2 wt%, only). This result is in line with the

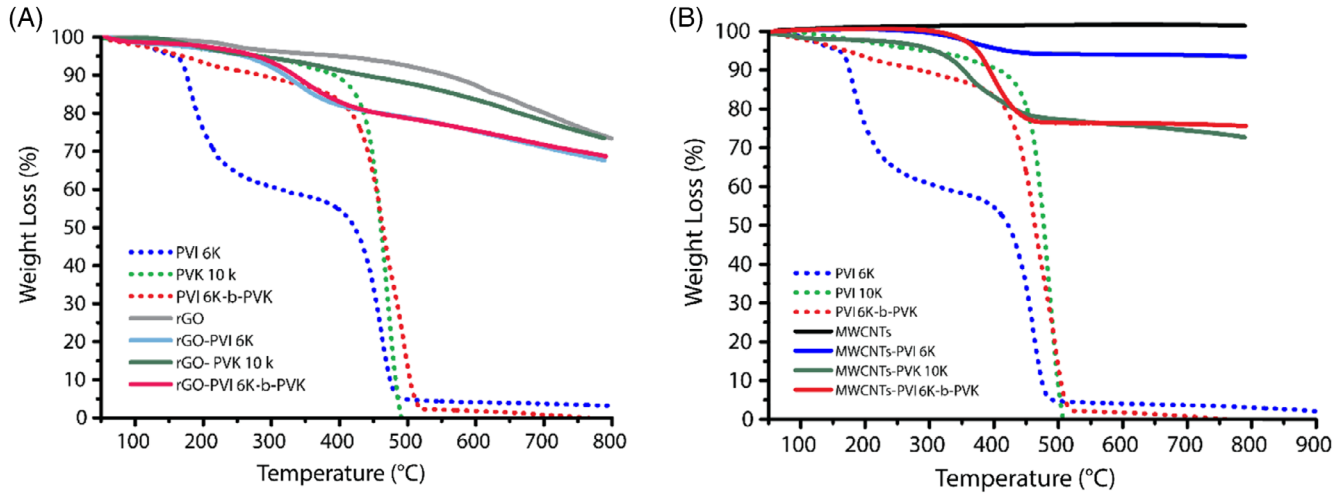


**FIGURE 5** TGA analysis of pristine polymers synthesized in this work and their composites. In the specific (A) reports TGA analysis of nanocomposites with GO and (B) reports TGA analysis of nanocomposites with MWCNTs

**TABLE 2** Summary of the amount of PVI 6 k, PVK 10 k and PVI 6 k-*b*-VK interacting with the filler at the end of the dispersion procedure

| | Polymer (wt%) | | |
|---|---|---|---|
| **GF** | **PVI 6 k** | **PVK 10 k** | **PVI 6 k-*b*-PVK** |
| rGO | 10.9 | 1.2 | 7.2 |
| MWCNTs | 8.0 | 28.7 | 25.8 |

data obtained by the TGA of PVK 10 k that displays a strong ability to interact with MWCNTs.

It is possible to explain the results considering the nature of the interactions between the GF and the polymers. rGO contains residual polar groups at its surface, providing a better interaction with the PVI moieties for MWCNTs. On the other hand, MWCNTs being characterized by a more graphitic character than rGO, effectively enabling the formation of $\pi$-$\pi$ interactions with the carbazole groups of PVI 6 k-*b*-PVK, analogous to reports of other aromatic compounds.[66–68] Those considerations seem to be confirmed by SEM analysis of the nanocomposites with rGO and MWCNTs (Figure 6). When rGO is used as GF, no remarkable differences are observed in the homogeneity of the filler dispersion in PVI 6 k (Figure 6A) and (PVI 6 k-*b*-VK; Figure 6B). On the contrary, it is possible to see a more homogenous dispersion of MWCNTs without bundles when PVI 6 k-*b*-PVK is used as polymer matrix (Figure 6D) instead of PVI 6 k (Figure 6C).

It is also interesting to note that both SEM micrographs of PVI 6 k-*b*-PVK show the presence of, most probably, polymer nanoparticles having a radius of ~20 nm. Such assemblies are possibly formed by PVK domains that are phase-separated from PVI due to the different nature and polarity of the two blocks. However, further investigations are needed before drawing a final conclusion. It is important to highlight that Raman spectra carried on the GF before and after the dispersion in the polymer matrix display no variation in the D/G band ratio (Figure S16). This confirms that the condition used for the dispersion of the GF did not adversely affect the graphitic nature of the GF fillers.

The ability to efficiently disperse GF was then evaluated by determining the percolation threshold in solid composites. The electrical behavior of the solid composite was evaluated by depositing the dispersion via solution casting over an electrical circuit (Figure S2). The device was then connected to a digital multimeter with a data logger. Since the resistance of the composite containing rGO (Figure S16) was considered too high due to the low conductivity of the filler (around GΩ, possibly due to the mostly intact insulating GO structure), further discussion was addressed only to the solid dispersions containing MWCNTs, only. Interesting results were obtained from the comparison of the MWCNTs-solid dispersion in the different polymers. The solid mixture based on MWCNTs dispersed in PVI 6 k displays the highest percolation threshold of about 1 wt%, whereas the PVI 6 k-*b*-PVK and PVK 10 k composites containing the more interacting VK units show the formation of effective percolation pathways already at MWCNTs contents of 0.5–0.7 wt% (Figure 7).

It is possible to conclude that the lower percolation threshold measured in the case of the copolymers reflects the higher interaction features of the polymer matrix with the MWCNTs, thus confirming the initial hypothesis of this work about the affinity of VK with MWCNTs.

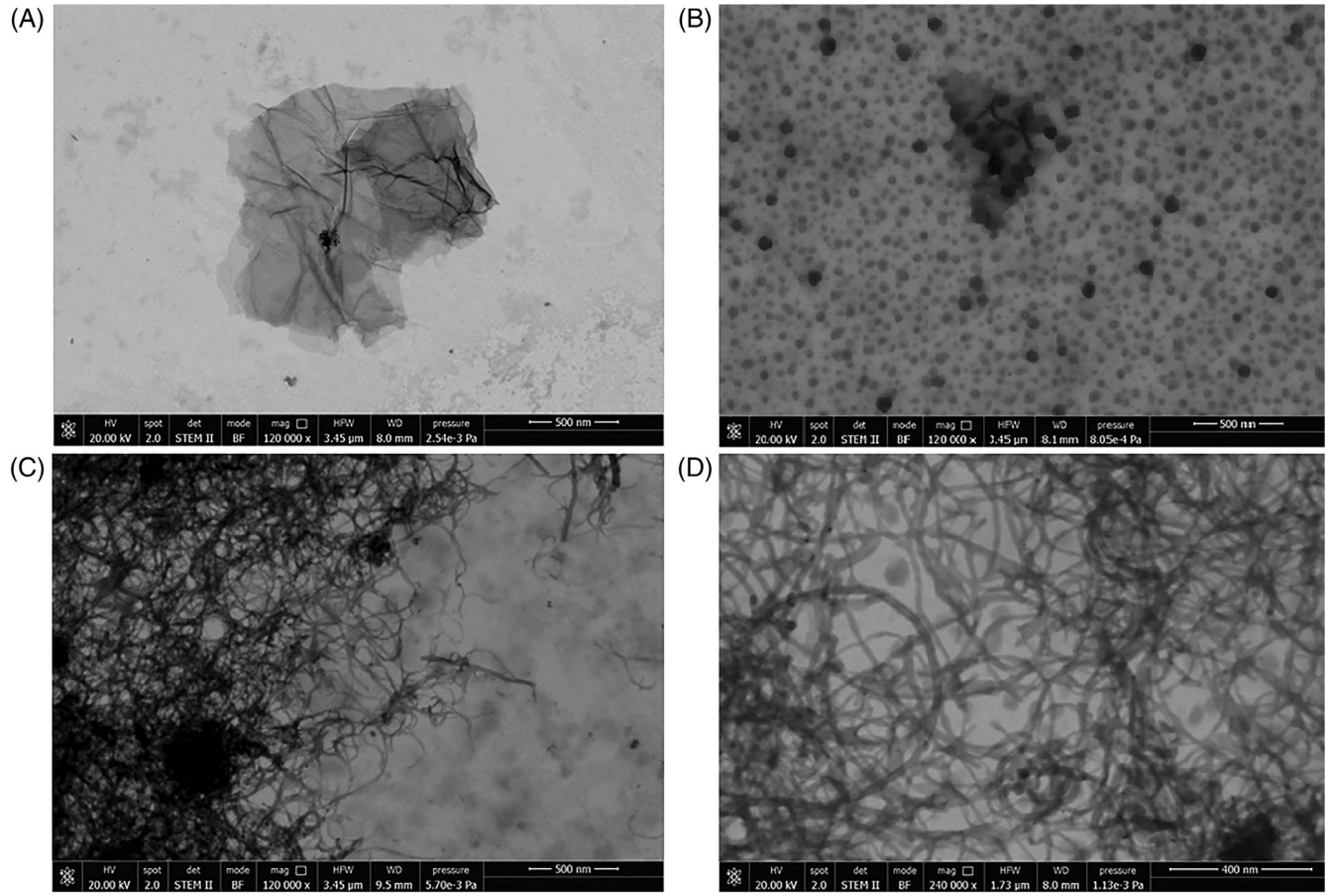


FIGURE 6 SEM images of the nanocomposites at 1 wt% of GF synthesized in this work. (A) PVI 6 k 1 wt% rGO. (B) PVI 6 k-*b*-PVK 1 wt% rGO. (C) PVI 6 k 1 wt% MWCNTs. (D) PVI 6 k-*b*-PVK 1 wt% MWCNTs

## 2.3 | Resistance responsiveness of the MWCNTs-composites with organic chemicals

Since the MWCNTs nanocomposites showed higher conductivity and lower percolation threshold, they were chosen as resistive composites for testing their potential interaction with chemicals. Organic solvents and acids were tested to determine the resistance response of the derived composites. The amount of 1 wt% of GF was chosen for the experiments being close to the percolation threshold and therefore suitable for resistive sensing.[69] The device coated with the nanocomposites was immersed in different organic solvents at room temperature for about 1 min. No polymer leakage from the solid support nor dissolution occurred during the sensing experiments. Notably, the prepared polymers resulted soluble in certain organic solvents after heating, only. From this first experiment, interesting results can be observed (Figure 8). When PVK 10 k was immersed in chlorinated solvents ($CHCl_3$ and $CH_2Cl_2$) and THF, a higher resistance variation was recorded in the nanocomposites. This behavior can be

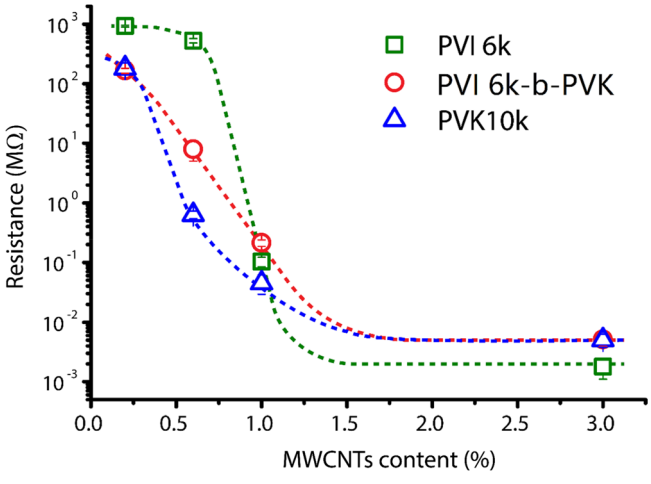


FIGURE 7 Percolation threshold of MWCNTs nanocomposites with PVI 6 k and PVI 6 k-*b*-PVK

possibly attributed to the high affinity of the VK repeating units with this class of solvents characterized by the highest polarity index (i.e., $CHCl_3$ = 4.1, $CH_2Cl_2$ = 3.1, and THF = 4.0).[70] The high interaction allows substantial

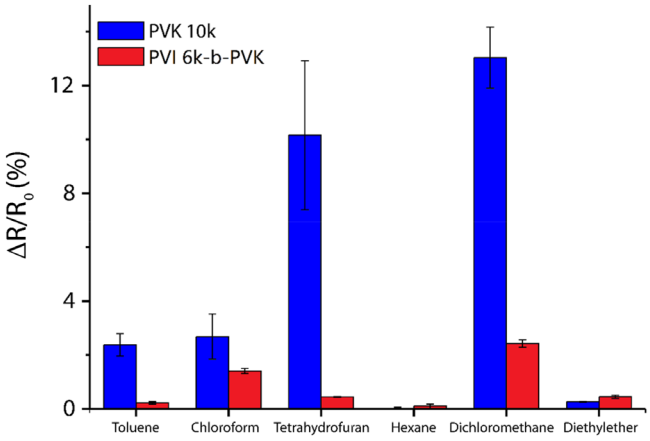


**FIGURE 8** Resistance variation of the sensor composed by PVI 6 k-*b*-PVK or PVK 10 k and 1 wt% of MWCNTs when immersed in organic solvents

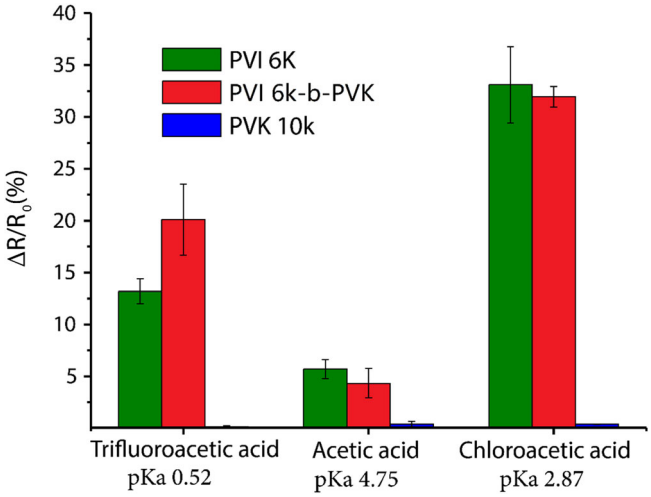


**FIGURE 9** Resistance variation of the sensor composed of PVI 6 k, or PVI 6 k-*b*-PVK or PVK 10 k and 1 wt% of MWCNTs when immersed in 0.2 M organic acids in toluene

swelling that adversely affect the percolative pathways of the composite and, in turn, results in an increase of electrical resistance.[71] In the case of PVI 6 k-*b*-PVK, the presence of the VI block dilutes the amount of PVK block, thus providing a less pronounced resistance variation, albeit the same trend. The highest sensitivity displayed by using dichloromethane is very promising for further investigations of the prepared device as sensors, for example, of volatile organic compounds.

The presence of imidazole moieties in the copolymer suggests testing the resistive response also towards organic acid compounds. In view of lack of solubility in solvents with lowest resistive response (Figure 8), the experiments were carried out by using toluene. This enabled the use of three different acid compounds with an increasing pKa (i.e., trifluoroacetic acid > chloroacetic acid > acetic acid) and without a detrimental interference due to the solvent, especially in the case of PVI 6 k-*b*-PVK, as resulted by preliminary experimental test.

Interesting results are obtained from the acid sensitivity of the composites. As expected, the PVK 10 k composite does not display any detectable resistance variation (Figure 9) since it cannot be protonated. It is likely that by protonating the VI, the resistance value of the derived composites changes significantly. It was expected that the stronger the acid, the more pronounced was the resistance variation. Conversely, the experimental data shows an unexpected behavior, as the chloroacetic acid (pKa = 2.87) gives the highest average resistance variation than that provided by the trifluoroacetic acid (pKa = 0.52).

This phenomenon was tentatively attributed to the stronger interaction of chlorinated compounds with the polymer matrices. Namely, notwithstanding the lower acid constant, the chloroacetic acid, thanks to its higher affinity with the polymer matrix, could diffuse within the solid MWCNTs/polymer mixture and reach a higher amount of VI moieties. Overall, the protonation adversely affects the electrical conductivity of the composites, possibly due to charge repulsion among macromolecules that tend to keep apart the electrically conductive MWCNTs.[36] No striking differences between the resistive behavior of PVI 6 k-*b*-PVK or PVK 10 k are present except for TFA, where the higher compatibility provided by the VK units towards the strongest acid could be beneficial in enhancing the responsiveness of the copolymer. Moreover, the acid-treated devices were unaffected by the presence of bases. For example, no variation of resistance occurred by adding highly concentrated DABCO (pKa is 8.82) solutions in toluene.

## 3 | CONCLUSION

In this work, block copolymers of 1-vinylimidazole and 9-(vinylcarbazole) have been successfully synthesized by RAFT polymerization for the first time. The products were extensively characterized by GPC, $^1$H-NMR, TGA, DSC, and UV–Vis. The monomer conversion was followed over the course of the polymerization, showing the expected pseudo-first-order kinetics, and GPC traces confirm continuously increasing molecular weights with moderate dispersity for the polymers, suggesting a certain degree of control. The synthesis of both macroRAFT agents (PVI and PVK) with different molecular weights was achieved. The greater $Đ$ for the PVI was likely due to the high conversion values (>60%) achieved.[60] When both macroRAFT agents were chain-extended, only PVI gave an acceptable result due to precipitation in case of PVK. However, the final

dispersity of the block copolymers was less than optimal for RAFT polymerization. This can be attributed probably to the poor livingness of the starting RAFT macro-initiators used. Fluorescence measurements of the synthesized copolymers were in agreement with literature reports for carbazole-containing polymers.[62] Since the carbazole is directly attached to the polymer backbone, the presence of a mainly "sandwich-like" conformation fluorescent excimer is registered in liquid and in solid-state. Two different GF were tested to prepare responsive conductive composites, rGO and MWCNTs, with the latter showing better interaction with the PVI-*b*-PVK, due to the different polar affinity with PVI-*b*-PVK compared to the rGO. Moreover, when SEM analyzed the responsive conductive nanocomposites with MWCNTs, it is clear that the use of PVK as second block help to prevent the formation MWCNTs bundles. Moreover, the GF's scavenging characteristics help improve the thermal stability of the polymers up to 350 °C. The CNTs show a low percolation threshold (∼ 0.85 wt%) due to the good non-covalent interaction with VK. Indeed, nanocomposites of PVI display a much higher percolation threshold value as proof of the inefficient ability of the VI to exfoliate MWCNTs.

Finally, the composites were tested in terms of electrical response when exposed to organic acid and chlorinated solvents to evaluate them for possible use in sensing devices. They showed good selectivity for different organic solvents, especially those based on the PVK 10 k homopolymer, with DCM and THF giving significantly higher variation than other solvents. This is a good starting point for further studies. On the other hand, the block copolymers display sensitivity and selectivity to organic acids due to the presence of the basic VI block, further expanding the possible practical applications.

## 4 | EXPERIMENTAL SECTION

### 4.1 | Materials

2-Butylthiocarbonothioylthio propanoate trithiocarbonate (MCEBTTC) was synthesized according to the procedure reported in the supporting information of this paper. 1-Vinylimidazole (VI, Sigma-Aldrich, ≥99%) was purified by filtration over basic alumina. Carbon disulfide (Sigma-Aldrich, anhydrous, ≥99%), 1-butanethiol (Sigma-Aldrich, 99%), methyl 2-bromopropionate (Sigma-Aldrich, 98%), 9-vinylcarbazole (VK, Sigma-Aldrich, 98%), 1,3,5 trioxane (Sigma-Aldrich, 99%), 2,2′-azobis(2-methylpropionitrile) (AIBN, Sigma-Aldrich, 98%), triethylamine (Sigma-Aldrich, ≥99%), magnesium sulfate (Sigma-Aldrich, anhydrous, ReagentPlus®, ≥99.5%), hydrochloric acid (ACS reagent, 37%), acetic acid (Sigma-Aldrich, glacial, ReagentPlus®, ≥99%), *N*,*N*-dimethylformamide (DMF, Sigma-Aldrich, for HPLC, ≥99.9%), diethyl ether (Sigma-Aldrich, anhydrous, ≥ 99.8%), dichloromethane (Sigma-Aldrich, for HPLC, ≥99.9%), trifluoroacetic acid (Sigma-Aldrich, ReagentPlus®, 99%), toluene (Sigma-Aldrich, ACS Reagent, ≥99.7%), hexane (Sigma-Aldrich, for HPLC, ≥97.0%), dimethyl sulfoxide (DMSO, Sigma-Aldrich, dried ≤0.02% water), 1-methyl-2-pyrrolidinone (NVP, Sigma-Aldrich, ReagentPlus®, 99%), tetrahydrofuran (THF, Carlo Erba), chloroacetic acid (Sigma-Aldrich, ACS reagent, ≥99.0%) were used as received. Reduced graphene oxide (rGO, Abalonyx, R-9P, by ELEM. ANAL: C 68.84%, H 1.41%, O 29.14%, and N 0.48%), Multi-Walled Carbon Nanotube (MWCNTs, Aldrich, as-produced cathode deposit, >7,5%) were used as GF. Dimethyl sulfoxide-$d_6$ (DMSO-$d_6$, Sigma-Aldrich, anhydrous, 99.9 atom % D) and chloroform-$d_3$ ($CDCl_3$, Sigma-Aldrich 99.8 atom%D) were used as deuterated solvents for NMR studies.

### 4.2 | General procedure for the synthesis of poly(1-vinylimidazole) and poly (9-vinylcarbazole) macroRAFT agents

The monomer (VI or VK; Scheme 1), MCEBTTC, AIBN and 1,3,5-trioxane (as an $^1$H-NMR internal reference, 1.5 wt% compared to the monomer) were dissolved in the reaction solvent (acetic acid for VI polymerization and 1,4-dioxane for VK polymerization) to a final monomer concentration of 1.6 M and transferred in a three-necked round-bottom flask according to the stoichiometric ratio reported in Table 1. The solution was purged with argon for 45 min and then submerged in an oil bath at 70 °C (in the case of PVI) and 60 °C (in the case of PVK; Table 1). Aliquots of the reaction solution were taken in regular time intervals to follow the reaction kinetics and analyzed by GPC and $^1$H-NMR spectroscopy. The reaction was stopped by cooling the reaction mixture to room temperature and opening the flask to air. The monomer conversion was determined via $^1$H-NMR spectroscopy by dissolving crude solution in DMSO-$d_6$ (PVI) or $CDCl_3$ (PVK). The PVI solutions were dialyzed against MilliQ water, changing the water at least three times over a period of 2 days, using a Spectrum™ Spectra/Por™ RC membrane with a 3.5 kDa molecular weight cut-off value. The final PVI macroRAFT agents were recovered as yellowish solid by removing MilliQ water using a freeze drier. PVK was purified by precipitating the solutions in cold diethyl ether. The final PVK macroRAFT agents were recovered by filtration as yellowish solids and dried overnight in a vacuum oven at 40 °C. All the products were characterized by $^1$H-NMR spectroscopy and GPC.

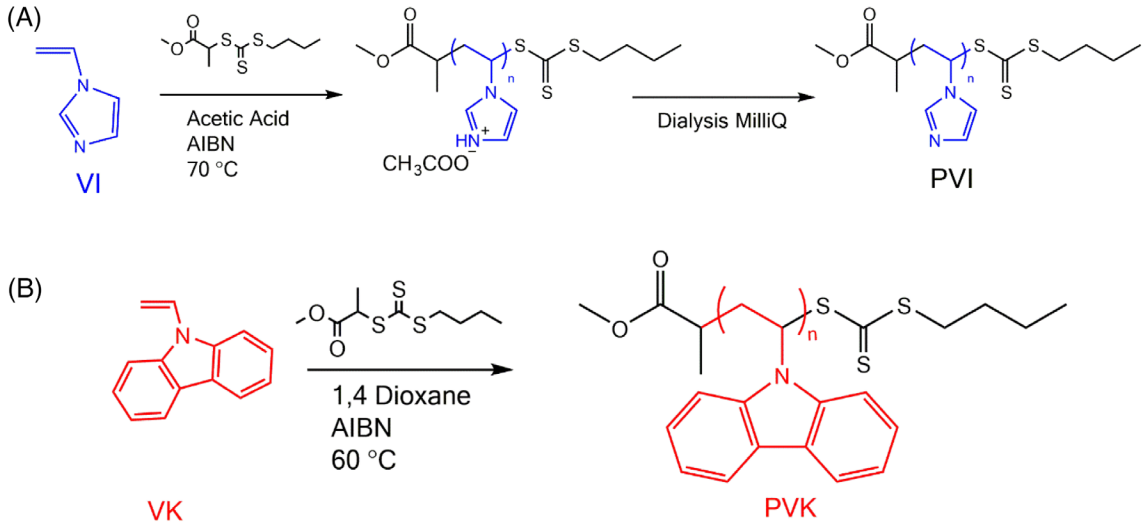


SCHEME 1 (A) Polymerization of VI in acetic acid followed by dialysis in MilliQ to obtain PVI macroRAFT agents. (B) Polymerization of VK to obtain PVK macroRAFT agent with different molecular weights

### 4.3 | Synthesis of PVI-*b*-PVK using thermo-initiated RAFT

According to the following procedure, the synthesis of PVI-*b*-PVK (Scheme 2) with different ratios of VI/VK was carried out. PVI macroRAFT, VK, and AIBN (according to the stoichiometric ratio reported in Table 1) were dissolved in DMF to a final monomer concentration of 1 M and transferred in a three-necked round-bottom flask. The solution was purged with argon for 45 min and then placed in an oil bath at 70 °C for 23 h. The kinetics of the reaction was followed by $^1$H-NMR, dissolving the crude solution in DMSO-$d_6$. The polymer solutions were dialyzed against DMF, changing DMF at least two times over a period of 2 days, using a Spectrum™ Spectra/Por™ RC membrane with a 3.5 kDa molecular weight cut-off value. The final polymers were recovered by precipitation in diethyl ether. The final polymer was recovered by filtration, washed with THF, and recovered as a whitish solid. The polymers were dried overnight in a vacuum oven at 40 °C. The products were characterized by $^1$H-NMR spectroscopy and GPC.

### 4.4 | Interaction tests between GF and polymers

110 mg of PVI 6 k (where 6 k stands for 6 kg/mol), PVK 10 k (where 10 k stands for 10 kg/mol) or PVI 6 k-*b*-PVK were dissolved in 15 ml of NMP in a 20 ml vial and 30 mg of rGO or MWCNTs were added. The mixtures were then sonicated for 5 min at 400 W. During sonication, the vial was immersed in an ice bath preventing an excessive temperature rise. Then, the dispersion was transferred in a 50 ml round-bottom flask equipped with a condenser and a stirring bar. The mixture was left to stir for 24 h at 70 °C under nitrogen. After cooling, the carbonaceous-polymer dispersion was precipitated in 1 L of water dropwise and recovered via filtration using a Sartorius filter (Durapore®) with a PVDF filter membrane with a pore size of 0.22 μm and a diameter of 47 mm. The product was washed with 250 ml of DMSO to remove the unreacted polymer, left under stirring overnight and then filtrated. The procedure of washing was repeated twice. The carbonaceous-polymer products were then dried for 48 h under vacuum and characterized by Raman spectroscopy and TGA.

### 4.5 | Preparation of the different GF/polymer nanocomposite

Dispersions of 1 mg/ml of rGO or MWCNTs were prepared in NMP and sonicated for 5 min at 400 W and 24 kHz with UP 400 S titanium probe with a 3 mm diameter tip and 100 mm length (Hielscher's H3). During sonication, the vial was immersed in an ice bath preventing an excessive temperature rise (Figure S1). Then, 50 mg of the polymer was dissolved in 5 ml of NMP and the right amount of GF (rGO or MWCNTs) dispersed in NMP was added in order to reach 0.2, 0.6, 1 and 3 wt% with respect to the polymer, respectively. The mixture was then ultrasonicated (UP400S from Hielscher) for 5 min at full power (400 W, frequency of 24 kHz), dipping the vial in an ice bath to prevent solvent evaporation during sonication. The GF/polymer dispersions were left stirring at 80 °C under nitrogen and one aliquot (20 μl) was drop-

**SCHEME 2** Reaction scheme of chain extension of PVI with VK in DMF to obtain PVI-*b*-PVK with different ratios of VI/VK

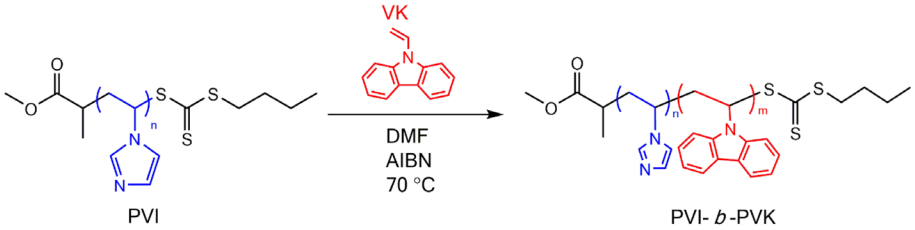


casted on copper plated electrodes supported on a Kapton® film[68] (Figure S2) and then left to evaporate at 120 °C. This procedure was repeated five times. After the last deposition, the device was left dried for 2 h at 120 °C and 6 h under low pressure (mechanical pump).

## 4.6 | Characterization

The $^1$H-NMR spectra were recorded on a Varian Mercury Plus 400 MHz spectrometer. TGA was carried out in a nitrogen environment with a PerkinElmer TGA 4000 from 20 to 900 °C at a heating rate of 10 °C/min. Glass transition temperatures ($T_g$) were determined for all samples using a TA-Instruments DSC25 under nitrogen atmosphere. $T_g$ was calculated as the point of inflection in the DSC curve. Two cycles were performed, and heating and cooling rates were set to 10 °C/min throughout the DSC measurements in the range of temperature of 15 °C to 280 °C according to the polymer measured.

The molecular weights of the polymers were measured by GPC analysis. The measurements were performed using several instruments with different solvent, depending on the polymer. The series of PVK were measured with an HP1100 from Hewlett Packard, equipped with three 300 × 7.5 mm PLgel 3 μm MIXED-E columns in series. Detection was made with a GBC LC 1240 IR detector. The samples were prepared by dissolving the polymers in THF at 1 mg/ml concentrations and using toluene as the internal standard. The samples were eluted with THF at a flow rate of 1 ml/min, at a pressure of 140 bar. Molecular weights and dispersity ($Đ$) were determined using the software PSS WinGPC Unity from Polymer Standard Service. Polystyrene standards ($M_n$ = 1180, 2360, 4490, 9920, 19,720, 46,500, 96,000, and 188,700 Da) were used for calibration. The series of PVI were measured with Agilent Technologies 1200 Series, equipped with PLgel Mixed B 300 × 7.5 mm. Detection was achieved with a GBC LC 1240 IR detector. The samples were eluted with DMF with 10 mM of LiBr at a flow rate of 1 ml/min, at a pressure of 30 bar. Molecular weights and dispersity ($Đ$) were determined using the software PSS WinGPC UniChrom V8.20. A standard pullulan kit (PSS, Mainz, Germany) with molecular weights from 342 to 805,000 Da was employed to generate a calibration curve. The molecular weights of the PVI-*b*-VK were measured using a GPC system consisting of an isocratic pump, auto sampler without temperature regulation, online degasser, 0.2-μm inline filter, refractive index detector (G1362A 1260 RID Agilent Technologies), viscometer (ETA-2010 PSS, Mainz), and MALLS detector (SLD 7000, PSS, Mainz). The samples were injected with a flow rate of 0.5 ml/min into a MZ Super-FG 100 SEC column and two PFG SEC columns 300 and 4000. The columns were held at 80 °C, and the detectors were held at 60 °C (Viscometer) and 45 °C (RI). A standard pullulan kit (PSS, Mainz, Germany) with molecular weights from 342 to 805,000 Da was employed to generate a calibration curve. The data were processed with the WinGPC Unity software (PSS, Mainz). The samples were dissolved in the GPC solvent DMSO with 50 mM LiBr at a concentration of 1 mg/ml by overnight stirring at room temperature. All samples were filtered through a 0.20-μm PTFE membrane before injected.

The fluorescence and absorbance spectra of the copolymers were measured both on solutions at 0.01 mg/ml in NMP, and on solid films. The polymer films were prepared by press molding at 1500 psi and using a temperature of 20 °C above their $T_g$ for 5 min. The fluorescence spectra were recorded on a Horiba Jobin–Yvon Fluorolog®-3 spectrofluorometric and the absorbance spectra on a Cary 5000 UV–Vis–NIR spectrophotometer. Scanning transmission electron microscopy (STEM) was performed using a FEI Quanta 450 ESEM FEG (ThermoFisher scientific, Hillsboro, Oregon, USA) with an accelerating voltage of 20 kV similar to procedures previously.[35] The percolation threshold of the various nanocomposites and the resistive behavior as a function of the different chemicals were determined by 2-point resistance measurement with a Solartron 7081 Precision Voltmeter, as analogously reported in previous experiments[36] Raman spectra were recorded on a BX51 upright microscope fiber coupled to a shamrock163i spectrograph and iVac-DR-316B-LDC-DD CCD camera (ANDOR Technology) with an 850-nm blazed 235 L/mm grating. An Ondax Mini-Benchtop Laser at 785 nm with 5 mW at sample.

## ACKNOWLEDGMENTS

The authors are grateful to Albert J. J. Woortman for GPC analysis and Prof. Dr. W.R. Browne for the RAMAN analysis of this work. NM is particularly grateful to Prof. Dr. W.R. Browne for the useful talk about the right interpretation of RAMAN analysis. CISUP—Centre for Instrumentation Sharing—University of Pisa is kindly acknowledged for STEM measurements.

## DATA AVAILABILITY STATEMENT

Data are available upon reasonable request to the corresponding author.

## ORCID

*Nicola Migliore* https://orcid.org/0000-0002-1314-1596
*Esteban Araya-Hermosilla* https://orcid.org/0000-0003-4271-6886
*Brent S. Sumerlin* https://orcid.org/0000-0001-5749-5444
*Andrea Pucci* https://orcid.org/0000-0003-1278-5004
*Patrizio Raffa* https://orcid.org/0000-0003-0738-3393

## REFERENCES

[1] D. Wang, Y. Jin, X. Zhu, D. Yan, *Prog. Polym. Sci.* **2017**, *64*, 114.
[2] H. Xie, K. K. Yang, Y. Z. Wang, *Prog. Polym. Sci.* **2019**, *95*, 32.
[3] H. Wang, J. Mei, P. Liu, K. Schmidt, G. Jiménez-Osés, S. Osuna, L. Fang, C. J. Tassone, A. P. Zoombelt, A. N. Sokolov, K. N. Houk, M. F. Toney, Z. Bao, *ACS Nano* **2013**, *7*, 2659.
[4] S. Hosseinzadeh, H. Hosseinzadeh, S. Pashaei, Z. Khodaparast, *Int. J. Biol. Macromol.* **2019**, *121*, 677.
[5] A. W. York, S. E. Kirkland, C. L. McCormick, *Adv. Drug Delivery Rev.* **2008**, *60*, 1018.
[6] S. Matsumura, A. R. Hlil, C. Lepiller, J. Gaudet, D. Guay, Z. Shi, S. Holdcroft, A. S. Hay, *J. Polym. Sci. Part A: Polym. Chem.* **2008**, *46*, 7207.
[7] S. A. Miners, A. Rance, A. N. Khlobystov, G. A. Rance, *Chem. Soc. Rev.* **2016**, *45*, 4727.
[8] J. Che, T. Çağin, W. A. Goddard, *Nanotechnology* **2000**, *11*, 65.
[9] H. C. Wu, X. Chang, L. Liu, F. Zhao, Y. Zhao, *J. Mater. Chem.* **2010**, *20*, 1036.
[10] Z. Deng, R. Yu, B. Guo, *Mater. Chem. Front.* **2021**, *5*, 2092.
[11] J. Chen, Y. Zhu, J. Huang, J. Zhang, D. Pan, J. Zhou, J. E. Ryu, A. Umar, Z. Guo, *Polym. Rev.* **2021**, *61*, 157.
[12] P. Lavrador, M. R. Esteves, V. M. Gaspar, J. F. Mano, *Adv. Funct. Mater.* **2021**, *31*, 1.
[13] O. Kanoun, A. Bouhamed, R. Ramalingame, J. R. Bautista-Quijano, D. Rajendran, A. Al-Hamry, *Sensors* **2021**, *21*, 1.
[14] V. Schroeder, S. Savagatrup, M. He, S. Lin, T. M. Swager, *Chem. Rev.* **2019**, *119*, 599.
[15] P. Zhao, M. Ni, C. Chen, Z. Zhou, X. Li, C. Li, Y. Xie, J. Fei, *Nanoscale* **2019**, *11*, 7394.
[16] M. Meyyappan, *Small* **2016**, *12*, 2118.
[17] S. Baik, H. J. Lee, D. W. Kim, J. W. Kim, Y. Lee, C. Pang, *Adv. Mater.* **2019**, *31*, 1.
[18] T. Alizadeh, S. Nayeri, S. Mirzaee, *Talanta* **2019**, *192*, 103.
[19] J. Chen, L. Yan, W. Song, D. Xu, *Compos. Part A: Appl. Sci. Manuf.* **2018**, *114*, 149.
[20] S. Kumar, A. Kumar, M. Kaur, D. Pal, K. Debnath, D. K. Aswal, A. Mahajan, *Sens. Actuators, B* **2021**, *327*, 128925.
[21] M. Turemis, D. Zappi, M. Teresa, G. Basile, A. Ramanaviciene, A. Kapralovs, A. Ramanavicius, R. Viter, *Talanta* **2020**, *211*, 120658.
[22] V. Shumeiko, E. Malach, Y. Helman, Y. Paltiel, G. Bisker, Z. Hayouka, O. Shoseyov, *Sens. Actuators, B* **2021**, *327*, 128832.
[23] S. Coiai, E. Passaglia, A. Pucci, G. Ruggeri, *Materials.* **2015**, *8*, 3377.
[24] T. Fujigaya, N. Nakashima, *Sci. Technol. Adv. Mater.* **2015**, *16*, 024802.
[25] Y. L. Liu, *Polym. J.* **2016**, *48*, 351.
[26] W. J. Lee, A. J. Clancy, J. C. Fernández-Toribio, D. B. Anthony, E. R. White, E. Solano, H. S. Leese, J. J. Vilatela, M. S. P. Shaffer, *Carbon N. Y.* **2019**, *146*, 162.
[27] T. Matrab, J. Chancolon, M. M. L'hermite, J. N. Rouzaud, G. Deniau, J. P. Boudou, M. M. Chehimi, M. Delamar, *Colloids Surfaces A Physicochem. Eng. Asp.* **2006**, *287*, 217.
[28] W. Ma, Y. Zhao, Z. Zhu, L. Guo, Z. Cao, Y. Xia, H. Yang, F. Gong, J. Zhong, *Appl. Sci.* **2019**, *9*, 603.
[29] S. Hosseinzadeh, H. Hosseinzadeh, S. Pashaei, Z. Khodaparast, *Ecotoxicol. Environ. Saf.* **2018**, *161*, 34.
[30] H. Hosseinzadeh, S. Pashaei, S. Hosseinzadeh, Z. Khodaparast, S. Ramin, Y. Saadat, *Sci. Total Environ.* **2018**, *640–641*, 303.
[31] P. Bilalis, D. Katsigiannopoulos, A. Avgeropoulos, G. Sakellariou, *RSC Adv.* **2014**, *4*, 2911.
[32] A. Xie, Y. Wang, P. Jiang, S. Li, X. Huang, *Compos. Sci. Technol.* **2018**, *154*, 154.
[33] S. Song, S. Xia, Y. Wei, X. Lv, S. Sun, Q. Li, *Macromol. Mater. Eng.* **2019**, *304*, 1.
[34] N. Migliore, L. M. Polgar, R. Araya-Hermosilla, F. Picchioni, P. Raffa, A. Pucci, *Polymer* **2018**, *10*, 618.
[35] F. Di Sacco, A. Pucci, P. Raffa, *Nanomaterials* **2019**, *9*, 458.
[36] F. Den Hoed, A. Pucci, F. Picchioni, P. Raffa, *Nanomaterials* **2019**, *9*, 1.
[37] K. M. Cui, M. C. Tria, R. Pernites, C. A. Binag, R. C. Advincula, A. C. S. Appl, *Mater. Interfaces.* **2011**, *3*, 2300.
[38] C. M. Santos, M. C. R. Tria, R. A. M. V. Vergara, F. Ahmed, R. C. Advincula, D. F. Rodrigues, *Chem. Commun.* **2011**, *47*, 8892.
[39] J. Zhang, Y. L. Luo, F. Xu, Y. S. Chen, *Chem. Eng. J.* **2016**, *298*, 136.
[40] R. S. Lee, H. J. Kim, J. E. Fischer, A. Thess, R. E. Smalley, *Nature* **1997**, *388*, 255.
[41] A. M. Rao, P. C. Eklund, S. Bandow, A. Thess, R. E. Smalley, *Nature* **1997**, *388*, 257.
[42] H. Aydin, B. Gündüz, C. Aydin, *Synth. Met.* **2019**, *252*, 1.
[43] M. Ates, M. Yildirim, O. Kuzgun, H. Ozkan, *J. Alloys Compd.* **2019**, *787*, 851.
[44] I. C. Mota, M. de Fátima, V. Marques, *Macromol. Symp.* **2019**, *383*, 1.
[45] J. Cui, Z. Song, L. Xin, S. Zhao, Y. Yan, G. Liu, *Carbon N. Y.* **2016**, *99*, 249.
[46] W. Y. Jeon, Y. B. Choi, H. H. Kim, *Ultrason. Sonochem.* **2018**, *43*, 73.
[47] C. Taylor, G. Kenausis, I. Katakis, A. Heller, *J. Electroanal. Chem.* **1995**, *396*, 511.

[48] E. H. Duarte, J. Casarin, E. R. Sartori, C. R. T. Tarley, *B Chem.* **2018**, *255*, 166.
[49] G. Yildiz, N. Oztekin, A. Orbay, F. Senkal, *Food Chem.* **2014**, *152*, 245.
[50] H. Dang, Y. Li, H. Zou, S. Liu, *Dyes Pigm.* **2020**, *172*, 107804.
[51] K. Sato, F. Sato, M. Kumano, T. Kamijo, T. Sato, Y. Zhou, Y. Korchev, T. Fukuma, T. Fujimura, Y. Takahashi, *Electroanalysis* **2021**, *33*, 1.
[52] A. Arslan, S. Kiralp, L. Toppare, A. Bozkurt, *Langmuir* **2006**, *22*, 2912.
[53] H. Bessbousse, T. Rhlalou, J. F. Verchère, L. Lebrun, *Chem. Eng. J.* **2010**, *164*, 37.
[54] Y. Suzuki, H. Nishide, E. Tsuchida, *Macromolecules* **2000**, *33*, 2530.
[55] M. M. Fares, A. M. Al-Shboul, *J. Biomed. Mater. Res. - Part A.* **2012**, *100A*, 863.
[56] A. Piloni, C. Cao, C. J. Garvey, A. Walther, M. H. Stenzel, *Macromol. Chem. Phys.* **2019**, *220*, 1.
[57] S. Asayama, T. Sekine, H. Kawakami, S. Nagaoka, *Bioconjugate Chem.* **2007**, *18*, 1662.
[58] B. Wang, H. J. Liu, T. T. Jiang, Q. H. Li, Y. Chen, *Polymer* **2014**, *55*, 6036.
[59] M. J. Molina, M. R. Gómez-Antón, I. F. Piérola, *J. Phys. Chem. B.* **2007**, *111*, 12066.
[60] B. Fan, J. Wan, A. McKay, Z. Qu, S. H. Thang, *Polym. Chem.* **2020**, *11*, 5649.
[61] M. H. Allen, S. T. Hemp, A. E. Smith, T. E. Long, *Macromolecules* **2012**, *45*, 3669.
[62] A. Botta, S. Pragliola, C. Capacchione, A. Rubino, R. Liguori, A. De Girolamo Del, V. V. Mauro, *Eur. Polym. J.* **2017**, *88*, 246.
[63] L. Izzo, P. Lisa, O. Sacco, S. Pragliola, *Polymer* **2021**, *13*, 1.
[64] C. Zheng, X. Xiang, *J. Fluoresc.* **2019**, *29*, 1343.
[65] M. C. Costache, M. J. Heidecker, E. Manias, G. Camino, A. Frache, G. Beyer, R. K. Gupta, C. A. Wilkie, *Polymer* **2007**, *48*, 6532.
[66] C. Liang, B. Wang, J. Chen, Q. Yong, Y. Huang, B. Liao, *J. Phys. Chem. B.* **2017**, *121*, 8408.
[67] T. Biver, F. Criscitiello, F. Di Francesco, M. Minichino, T. Swager, A. Pucci, *RSC Adv.* **2015**, *5*, 65023.
[68] C. Ehli, G. M. A. Rahman, N. Jux, D. Balbinot, M. Guldi, F. Paolucci, M. Marcaccio, D. Paolucci, F. Zerbetto, S. Campidelli, M. Prato, *J. Am. Chem. Soc.* **2006**, *128*, 11222.
[69] E. Araya-Hermosilla, M. Minichino, V. Mattoli, A. Pucci, *Chemosensors.* **2020**, *8*, 1.
[70] L. R. Snyder, J. J. Kirkland, J. L. Glajch, *Pract. HPLC Method Dev.* **2012**, *3*, 721.
[71] M. Ehsani, P. Rahimi, Y. Joseph, *Sensors* **2021**, *21*, 3291.

## SUPPORTING INFORMATION

Additional supporting information may be found in the online version of the article at the publisher's website.

**How to cite this article:** N. Migliore, E. Araya-Hermosilla, G. M. Scheutz, B. S. Sumerlin, A. Pucci, P. Raffa, *J. Polym. Sci.* **2022**, *60*(4), 674. https://doi.org/10.1002/pol.20210736